Electronic Supplementaryas Information for "Preferential electrostatic interactions of phosphatidic acid with arginines"

Nidhin Thomas[1], Wesley Combs[1], Kranthi K. Mandadapu[2,3], Ashutosh Agrawal[1,*]

1 Department of Mechanical Engineering, University of Houston, Houston, TX 77204
2 Department of Chemical & Biomolecular Engineering, University of California, Berkeley, CA 94720, USA
3 Chemical Sciences Division, Lawrence Berkeley National Laboratory, CA 94720, USA

Corresponding author:
*** ashutosh@uh.edu**

Molecular dynamics simulations

We used CHARMM-GUI (1, 2) to create the atomistic systems. Here we outline additional details in addition to the description provided in the Methods section. We added 0.15 mM KCl salt to neutralize the simulation box. The temperature and the pressure of the simulation systems were maintained at 303K and 1 atm, respectively. Simulations were performed using GROMACS 2018.3 (3). CHARMM36m and CHARMM36 (4, 5) force fields were used throughout the simulations for protein and lipids respectively. Furthermore, TIP3P water model (6) was used along with CHARMM36 force field for ions. Energy minimization of the system was performed using the steepest descent method to bring the maximum force in the system down to less than 700 KJ/mol.nm. Energy minimization was followed by three sets of NVT and NPT equilibration cycles, respectively. Hydrogen bonds were constrained using the LINCS algorithm (7). Verlet cut-off scheme was used with a cut-off distance of 1.2 nm. Short-range electrostatic interactions were cut-off at 1.2 nm and long-range interactions were calculated using PME (8). Van der Waal's interactions were cut-off at 1.2 nm and a force-switch VdW modifier was used to reduce long-range VdW force to zero. Berendsen thermostat and barostat were used during the equilibration cycles with a time constant of 1.0 ps for temperature coupling and a time constant of 5.0 ps for pressure coupling. Semi-isotropic pressure coupling with different pressure coupling along z-direction was used throughout the simulation with compressibility of 4.5×10^{-5} bar^{-1}. During NVT and NPT equilibration cycles, C_α carbons of VSD and phosphorus atoms in lipids were restrained and later the restraint forces were reduced to zero in the production runs. The total NVT and NPT equilibration time for each system was 4.5 ns. The Nose-Hoover thermostat (9, 10) was used in the production runs with a time constant of 1.0 ps. In addition, Parrinello-Rahman pressure coupling (11) with 5.0 ps time constant and compressibility of 4.5×10^{-5} bar^{-1} was used to maintain the pressure at 10^5 bar. The 4.5 ns of equilibration and the first 200 ns of the production runs were discarded to account for the equilibration. The details of the equilibrium simulations are provided in Table S1.

POPA$^{(-2)}$ parameters

Partial charge distribution of POPA$^{(-2)}$ lipids used in the simulation were taken from the methylphosphate (dianionic) residue available in CHARMM36 (12). It was adjusted for the methyl group connecting to the glycerol backbone. The partial charge of the methyl carbon atom in methylphosphate group was -0.27 and for POPA$^{(-2)}$ it was adjusted to -0.18. The partial charge distribution in the rest of the atoms of the lipid was identical to that for the POPA$^{(-1)}$ lipid. The partial charges of atoms in the POPA$^{(-2)}$ headgroup is shown in Fig. S5.

Density maps of lipids around the VSD

2D density map of the oxygen atoms in the lipid phosphate group was computed using the 'gmx densmap' command. The figures were made from the density values obtained by computing the number of occurrences of the oxygen atoms in a single pixel throughout the sampling, and then dividing by the cross-sectional area of the pixel using the equation given below.

$$\rho_{\text{pixel}} = \langle \frac{\sum_{n=1}^{N_l} \delta(\mathbf{r_{pixel}} - \mathbf{r_n})}{A_{\text{pixel}}} \rangle \quad [S1]$$

where N_l is the number of lipid molecules in outer leaflet, $\mathbf{r_{pixel}}$ is the position vector of a pixel, $\mathbf{r_n}$ is the position vector of n^{th} lipid oxygen atom in the phosphate group, and A_{pixel} is the cross sectional area of the pixel. Since POPC(75):POPA(25), POPC(75):POPG(25), and POPC(75):POPI(25) bilayer systems have three times more POPC lipids than either POPA, POPG or POPI lipids, the number density of POPC lipids far away from the VSD is three times more than that of the anionic lipids. However, due to the preferential aggregation of POPA lipids around the S4 segment, we observe a higher number density of POPA lipids. A similar trend can be seen in the reproduction runs of the POPC(75): POPA(25) system as well.

Pulling simulations

After 1.5 microsecond long equilibrium simulations, anionic lipids aggregated in the vicinity of positively charged ARG side chains. Two specific regions were identified as the aggregation hotspots using the 2D density maps. The first hotspot was identified in between the side chains of R117 and R120. The second hotspot was identified close to the R123 residue. We identified the corresponding POPC, POPA$^{(-1)}$, POPG, POPI, and POPA$^{(-2)}$ lipids in these hotspots and extracted the structures from the equilibrium simulations. In the first set of pulling simulations, center of mass of the lipid phosphate headgroup was pulled from the center of mass of the R117-R120 side chains. We followed this approach to pull POPC, POPA$^{(-1)}$, POPG, POPI, and POPA$^{(-2)}$ lipids away from the first hotspot. In the second set of pulling simulations, the center of mass of the lipid phosphate headgroup of POPA$^{(-1)}$ or POPA$^{(-2)}$ was pulled from the center of mass of R123 side chain close to the second hotspot. The lipid headgroups were pulled in the plane lateral to the lipid-water interface (X-Y plane) in the direction of the vector connecting the pulling groups. The schematic representing the pulling simulations are shown in Fig. S8. During the pulling simulations, the protein backbone atoms were restrained with 1000 kJ.mol^{-1}.nm^{-2}. A three dimensional reaction coordinate system was chosen for the pulling simulation. The force constant corresponding to the primary reaction coordinate was 1500 kJ.mol^{-1}.nm^{-2}. The pulling rate along this direction was 0.0001 nm/ps. The force constant corresponding to the secondary and tertiary reaction coordinates was 500 kJ.mol^{-1}.nm^{-2} and the pulling rate was set to 0.0 nm/ps. The other MD parameters were identical to those used in the equilibrium production simulations.

Umbrella sampling simulations

We performed seven umbrella sampling simulations. The initial structure corresponding to each window for these simulations were taken from the pulling simulations. The windows were chosen such that the increment along the primary reaction coordinate was 0.1 nm. After extracting the frames, each window was simulated for 200 ns and the last 50 ns were chosen for the free energy calculations. The MD simulation parameters used for the umbrella sampling simulations were identical to those used in the equilibrium production simulations. In addition, parameters from the pulling simulations were chosen for the COM-pulling simulations. The pulling rate was modified to zero. The number of umbrella sampling windows for each simulations are listed in Table S2 and the corresponding sampling window histograms are provided in Fig. S9.

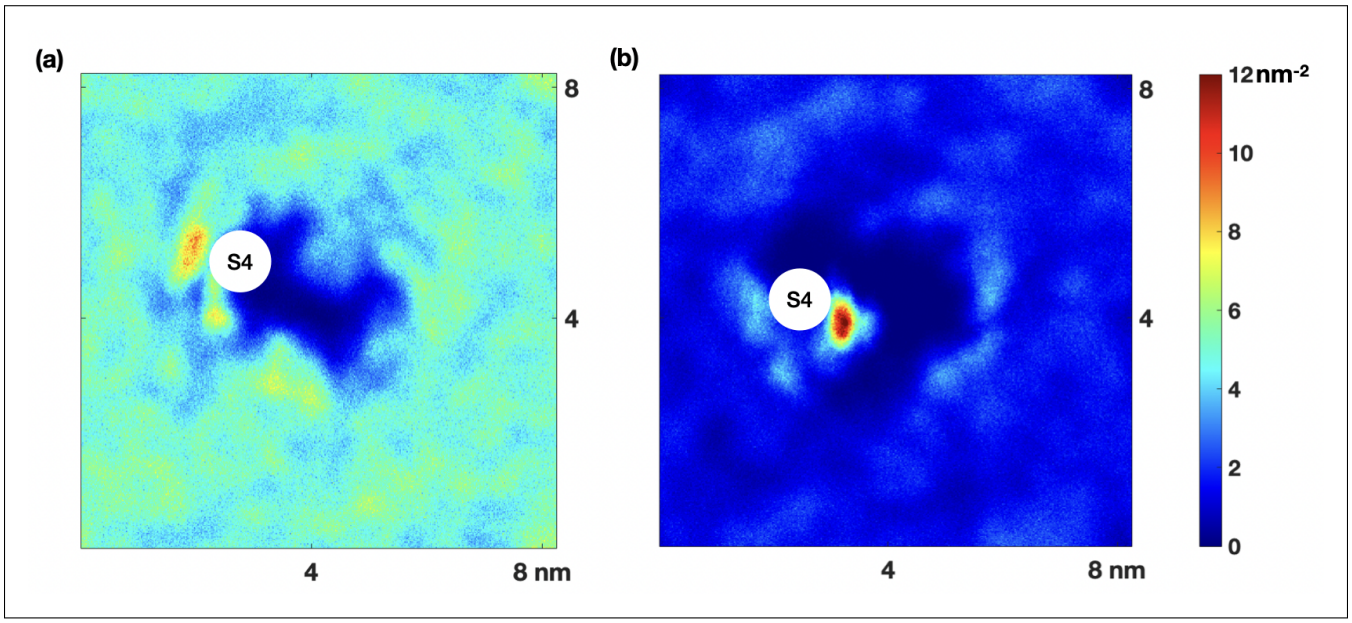

Figure S1: 2D number density plots from the additional simulations for **(a)** POPC and **(b)** POPA lipids in the extra-cellular leaflet of POPC (75): POPA (25) bilayer. The hotspot in the density around the S4 segment confirms preferential aggregation of POPA lipid around the ARG residues in the VSD. The color bar represents the total count of oxygen atoms in the phosphate group per nm^{-2}.

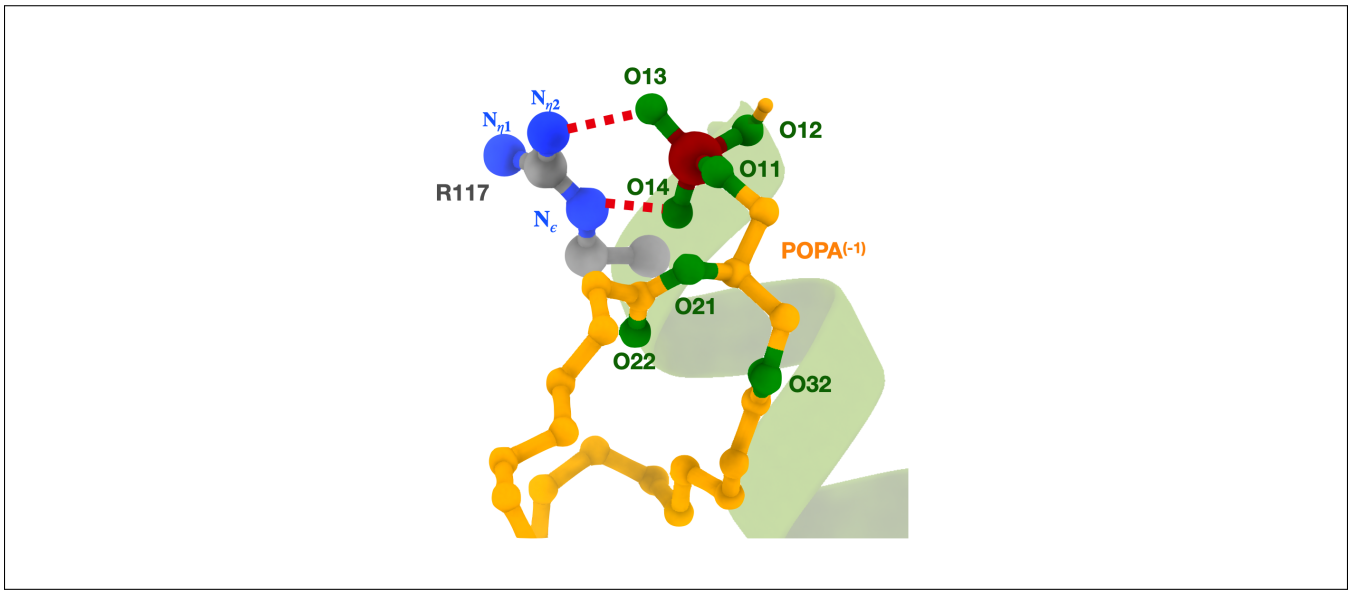

Figure S2: Electrostatic interactions between POPA lipid and ARG guanidinium side chain. Positively charged nitrogen atoms (N_ϵ, $N_{\eta 1}$, $N_{\eta 2}$) of guanidinium group are shown in blue. Negatively charged ester-linked oxygen (O11), hydroxyl oxygen (O12), and phosphate oxygen (O13, O14) atoms of lipid phosphate group are shown in green. The electrostatic interactions between the nitrogen atoms and the oxygen atoms are shown in red dashed lines.

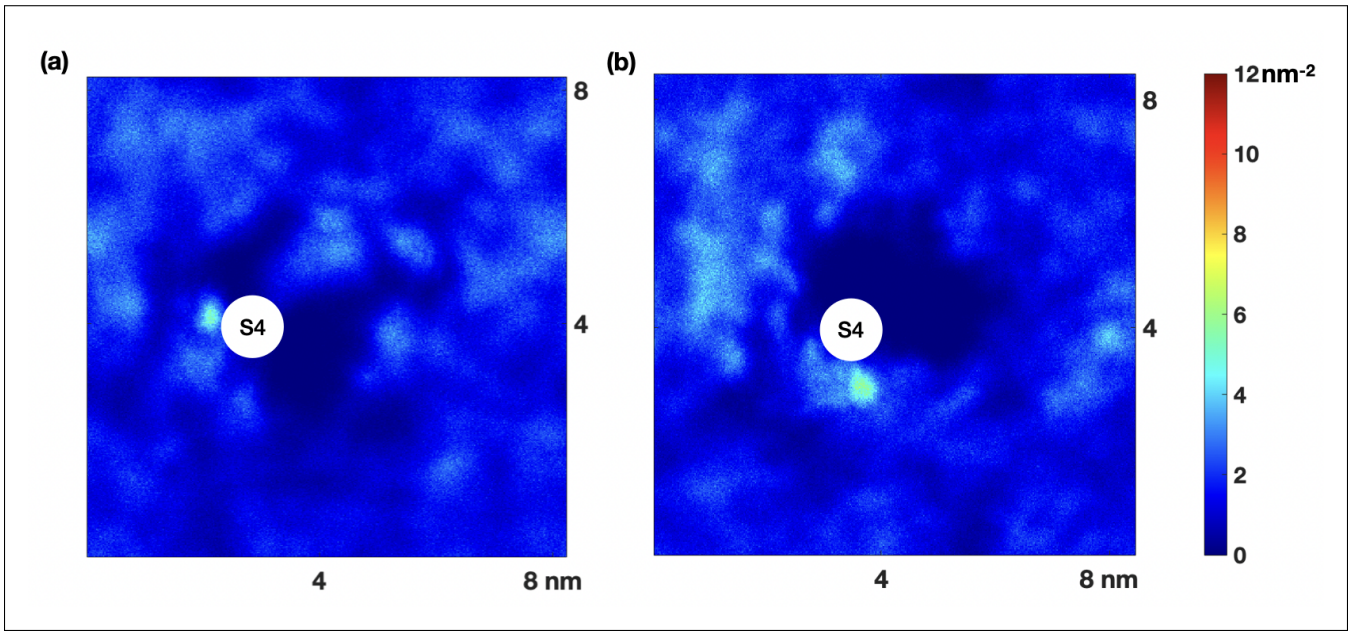

Figure S3: 2D number density plots from the additional simulations for **(a)** POPG lipids in the extra-cellular leaflet of the POPC (75): POPG (25) bilayer and **(b)** POPI lipids in the extra-cellular leaflet of the POPC (75): POPI (25) bilayer. The color bar represents the total count of oxygen atoms in the phosphate group per nm^{-2}.

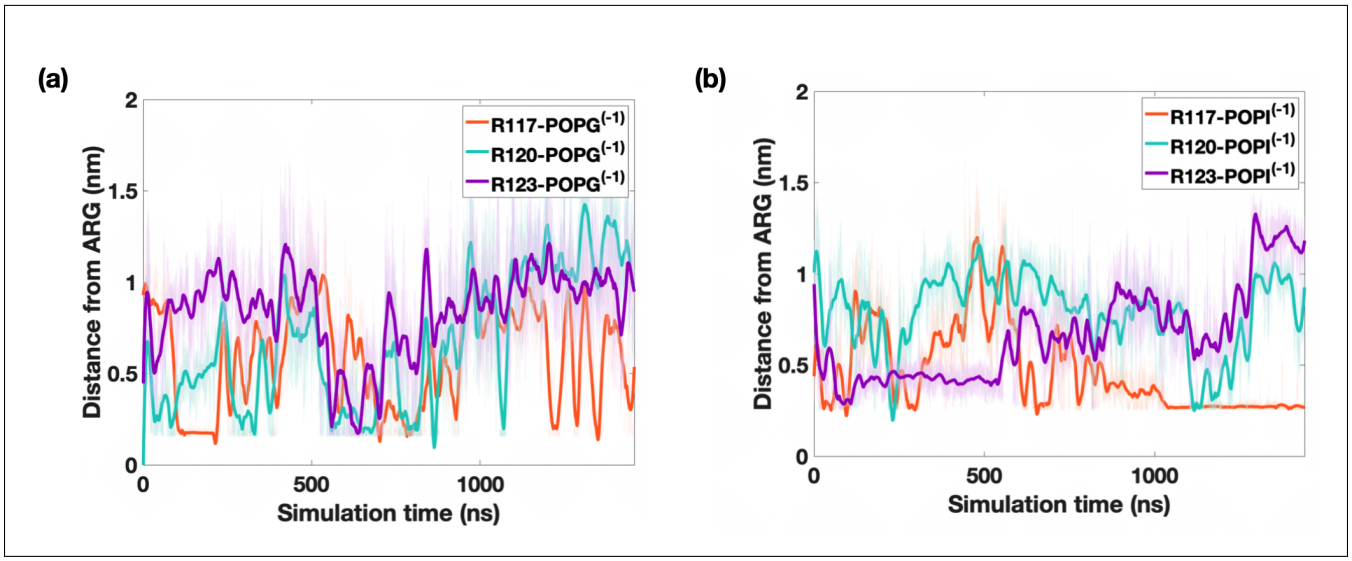

Figure S4: ARG-lipid distance time plots from the additional simulations for **(a)** POPG and **(b)** POPI systems. The large fluctuations in the plots suggest that the electrostatic interactions between the ARG side chains and the POPG/ POPI lipids are weaker in comparison to the POPA lipids. The weaker interactions could be attributed to the larger headgroup size of the POPG and POPI lipids.

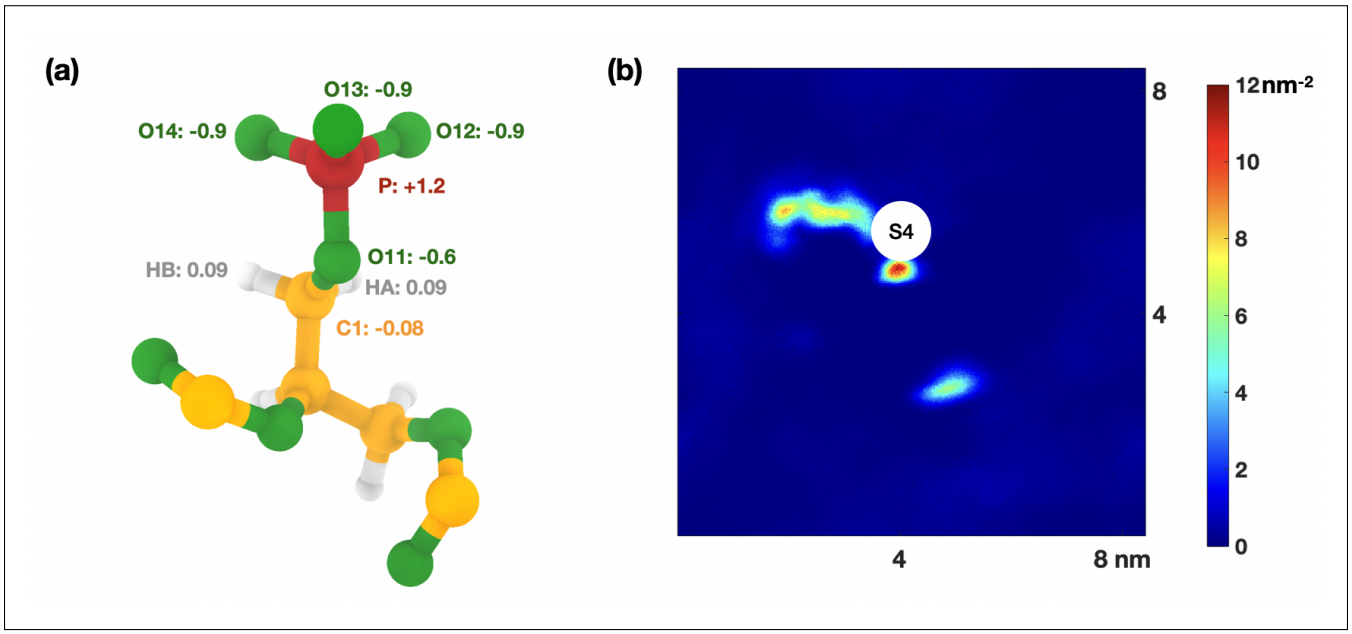

Figure S5: **(a)** Partial charge distribution of POPA$^{(-2)}$ lipids used in the simulation. The distribution was taken from the methylphosphate (dianionic) group available in CHARMM36 (12), adjusted for the methyl group connecting to the glycerol backbone. The partial charge of the methyl carbon atom in methylphosphate group was -0.27 and for POPA$^{(-2)}$ it was adjusted to -0.18. The partial charge distribution in the rest of the atoms of the lipid is identical to those for the POPA$^{(-1)}$ lipid. **(b)** 2D-density map of POPA$^{(-2)}$ lipids in the extra-cellular leaflet of the reproduction run. The peak in the density around S4 segment demonstrates preferential aggregation of POPA lipids around the S4 segment of the VSD.

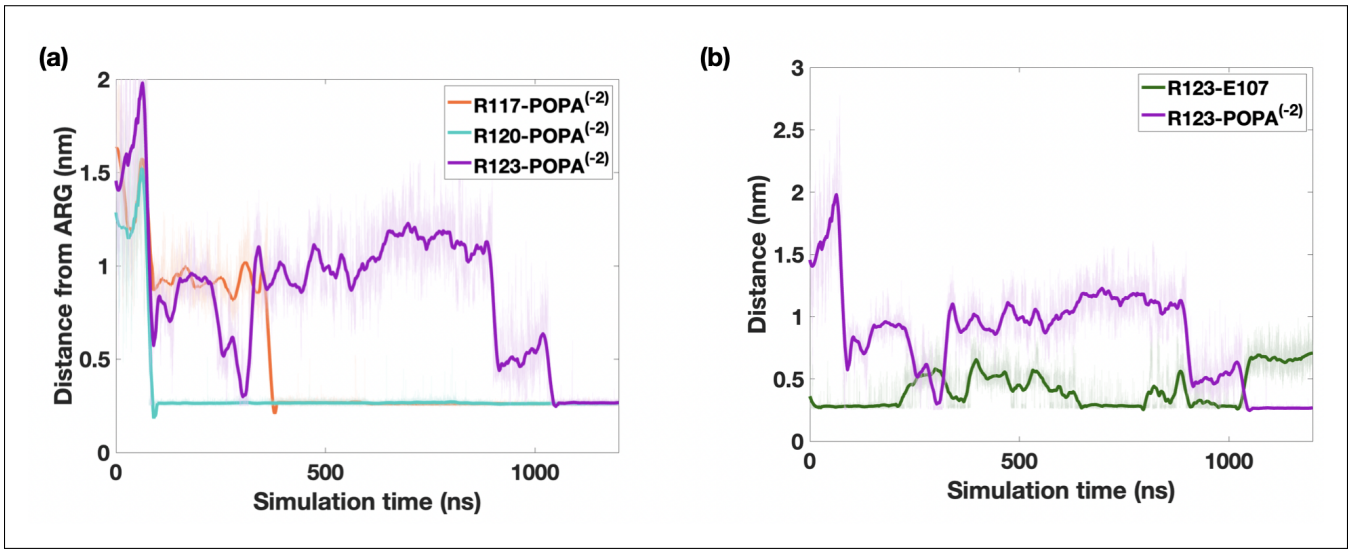

Figure S6: ARG-lipid distance time plots from the additional simulation for POPC: $POPA^{(-2)}$ system. **(a)** ARG-$POPA^{(-2)}$ distance-time plot shows that $POPA^{(-2)}$ lipids aggregate around the S4 ARG side chains. **(b)** The comparison of the R123-$POPA^{(-2)}$ and R123-E107 distance-time plots. It shows that the electrostatic interaction between the R123 and $POPA^{(-2)}$ headgroup breaks the salt bridge connection between R123 and E107 around 1000 ns.

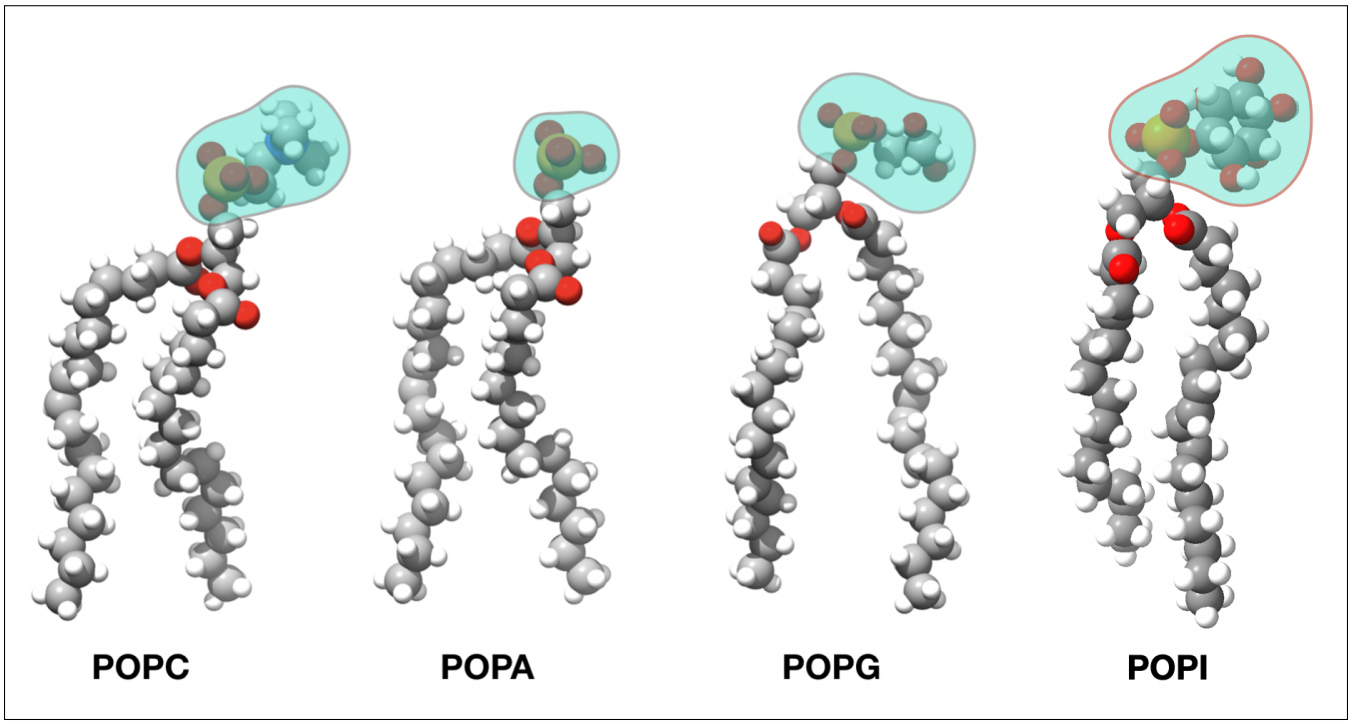

Figure S7: Comparison of the POPC, POPA, POPG, and POPI headgroup sizes. Volumetric footprint of the POPA headgroup is at least 35% smaller than those of the POPC, POPG or POPI lipids. This leads to a higher charge density in the POPA headgroup compared to other anionic lipids, which consequently should lead to stronger electrostatic interactions with the ARG residues of the S4 segment. Deprotonation of $POPA^{(-1)}$ lipid headgroup to $POPA^{(-2)}$ lipid would further increase the charge density for the POPA lipid.

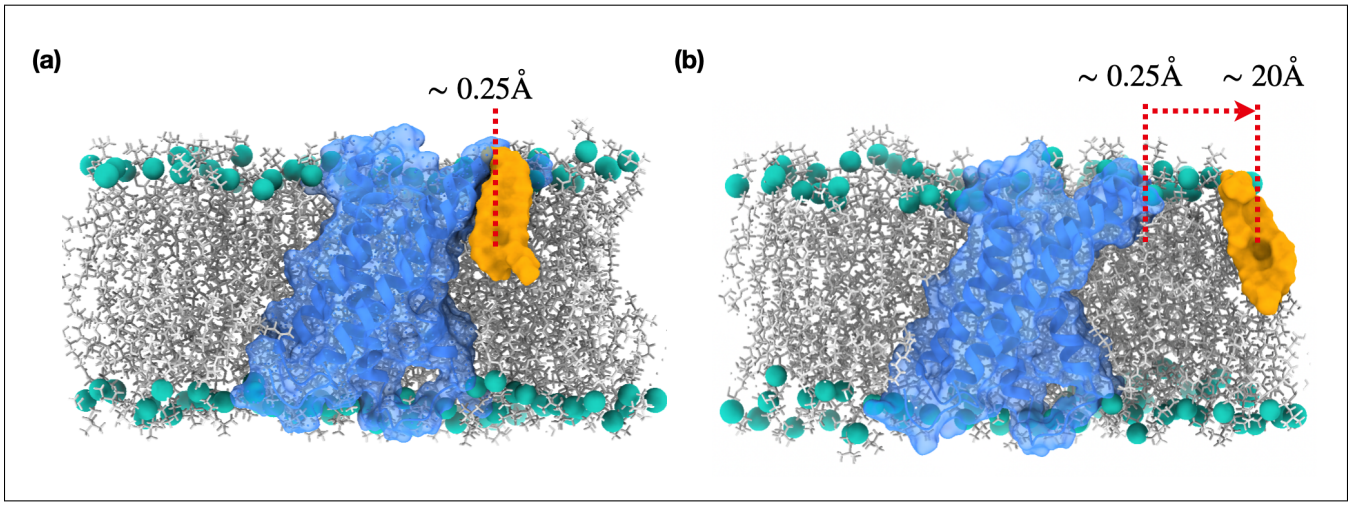

Figure S8: Schematic showing the procedure adopted for the pulling simulations to compute the free energy curves. We pulled the bound charged lipids lipids one-by-one away from the S4 segment in the outward radial direction in a sequence of steps and computed the free energy curves. This enabled us to compute the free energy gain offered by each lipid-arginine interactions

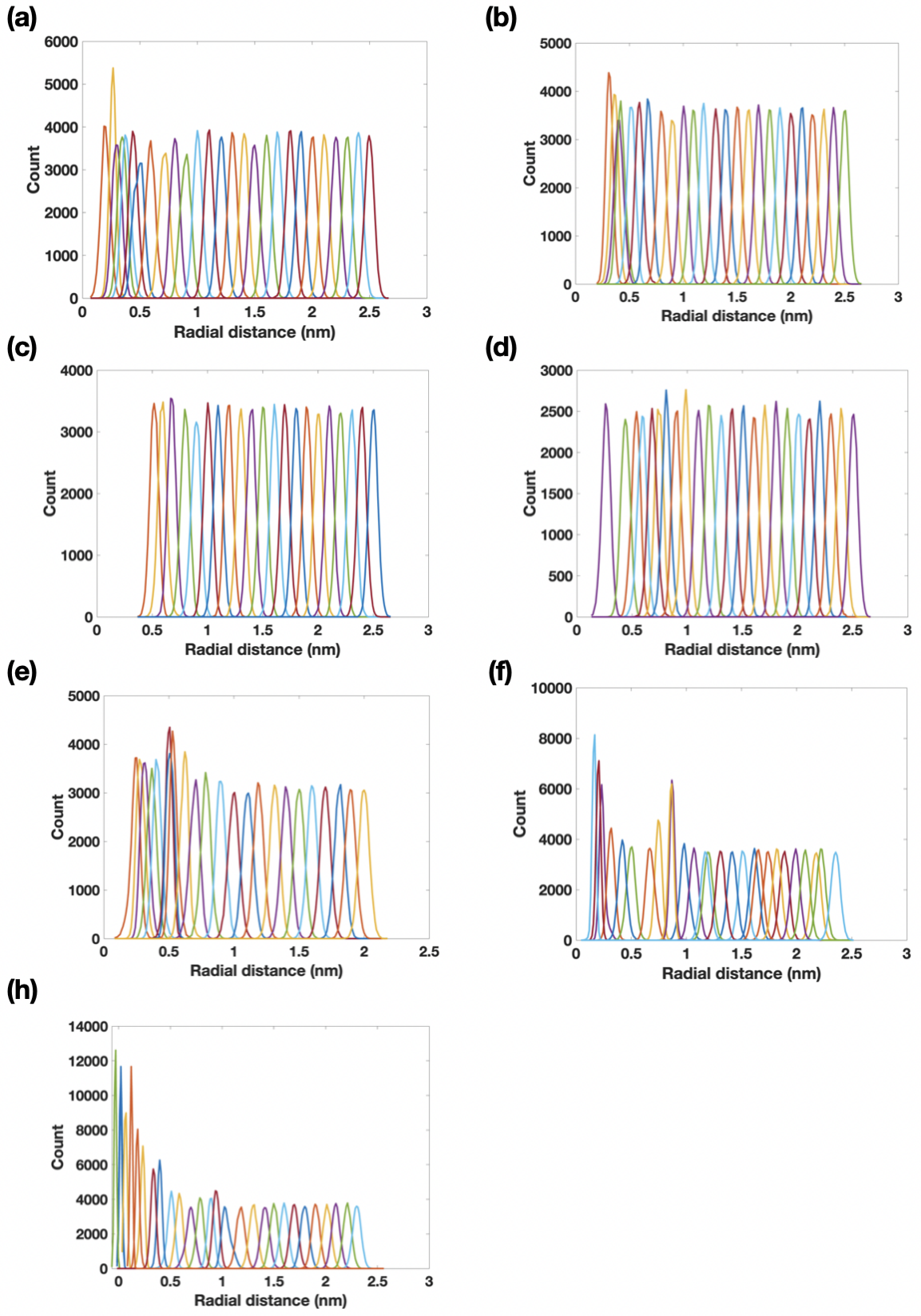

Figure S9: Umbrella sampling histograms for the **(a)** POPC, **(b)** POPA$^{(-1)}$-R117, **(c)** POPG-R117, **(d)** POPI-R117, **(e)** POPA$^{(-2)}$-R117, **(f)** POPA$^{(-1)}$-R123 and **(g)** POPA$^{(-2)}$-R123 systems.

Table S1: Summary of the equilibrium simulations performed in this study

Bilayer composition	**Lipids per leaflet**	**Simulation time (μs)**	**No. of runs**
POPC-Pure	POPC (200)	1.5	1
POPC-POPA$^{(-1)}$	POPC (75): POPA$^{(-1)}$ (25)	1.5	2
POPC-POPG	POPC (75): POPG (25)	1.5	2
POPC-POPI	POPC (75): POPI (25)	1.5	2
POPC-POPA$^{(-2)}$	POPC (90) : POPA$^{(-2)}$ (10)	1.5	2
POPC-DOPP$^{(-1)}$	POPC (90) : DOPP$^{(-1)}$ (10)	1.5	1
POPC-DOPP$^{(-2)}$	POPC (90) : DOPP$^{(-2)}$ (10)	1.5	1

Table S2: Summary of the umbrella sampling simulations performed in this study

Simulation ID	**Pulling lipid**	**No. of windows**	**Simulation time (ns)**
R117-POPC	POPC	28	200
R117-POPA$^{(-1)}$	POPA$^{(-1)}$	25	200
R117-POPG	POPG	25	200
R117-POPI	POPI	22	200
R117-POPA$^{(-2)}$	POPA$^{(-2)}$	24	200
R123-POPA$^{(-1)}$	POPA$^{(-1)}$	29	200
R123-POPA$^{(-2)}$	POPA$^{(-2)}$	27	200

References

1. Sunhwan Jo, Taehoon Kim, Vidyashankara G Iyer, and Wonpil Im. Charmm-gui: a web-based graphical user interface for charmm. *Journal of computational chemistry*, 29(11):1859–1865, 2008.

2. Sunhwan Jo, Joseph B Lim, Jeffery B Klauda, and Wonpil Im. Charmm-gui membrane builder for mixed bilayers and its application to yeast membranes. *Biophysical journal*, 97(1):50–58, 2009.

3. David Van Der Spoel, Erik Lindahl, Berk Hess, Gerrit Groenhof, Alan E Mark, and Herman JC Berendsen. Gromacs: fast, flexible, and free. *Journal of computational chemistry*, 26(16):1701–1718, 2005.

4. Jumin Lee, Xi Cheng, Jason M Swails, Min Sun Yeom, Peter K Eastman, Justin A Lemkul, Shuai Wei, Joshua Buckner, Jong Cheol Jeong, Yifei Qi, et al. Charmm-gui input generator for namd, gromacs, amber, openmm, and charmm/openmm simulations using the charmm36 additive force field. *Journal of chemical theory and computation*, 12(1):405–413, 2016.

5. Jing Huang, Sarah Rauscher, Grzegorz Nawrocki, Ting Ran, Michael Feig, Bert L de Groot, Helmut Grubmüller, and Alexander D MacKerell. Charmm36m: an improved force field for folded and intrinsically disordered proteins. *Nature methods*, 14(1):71–73, 2017.

6. Sander Boonstra, Patrick R Onck, and Erik van der Giessen. Charmm tip3p water model suppresses peptide folding by solvating the unfolded state. *The journal of physical chemistry B*, 120(15):3692–3698, 2016.

7. Berk Hess, Henk Bekker, Herman JC Berendsen, and Johannes GEM Fraaije. Lincs: a linear constraint solver for molecular simulations. *Journal of computational chemistry*, 18(12):1463–1472, 1997.

8. Tom Darden, Darrin York, and Lee Pedersen. Particle mesh ewald: An n log (n) method for ewald sums in large systems. *The Journal of chemical physics*, 98(12):10089–10092, 1993.

9. Shuichi Nosé and ML Klein. Constant pressure molecular dynamics for molecular systems. *Molecular Physics*, 50(5):1055–1076, 1983.

10. Shūichi Nosé. A molecular dynamics method for simulations in the canonical ensemble. *Molecular physics*, 52 (2):255–268, 1984.

11. Michele Parrinello and Aneesur Rahman. Polymorphic transitions in single crystals: A new molecular dynamics method. *Journal of Applied physics*, 52(12):7182–7190, 1981.

12. Jing Huang and Alexander D MacKerell Jr. Charmm36 all-atom additive protein force field: Validation based on comparison to nmr data. *Journal of computational chemistry*, 34(25):2135–2145, 2013.